Electronic Supplementary Material (ESI) for Physical Chemistry Chemical Physics.

ELECTRONIC SUPPPLEMENTARY INFORMATION

Formation of solid solution between $[N(C_2H_5)_4][BF_4]$ and $[N(C_2H_5)_4][PF_6]$ in the crystal and plastic crystal phases

Kazuhiko Matsumoto,* Ryojun Nonaka, Yushen Wang, Gleb Veryasov, Rika Hagiwara

Department of Fundamental Energy Science, Graduate School of Energy Science, Kyoto University

Sakyo-ku, Kyoto 606-8501, Japan

* E-mail: k-matsumoto@energy.kyoto-u.ac.jp

Table S1 Crystallographic data and refinement results for $[N_{2222}][BF_4]_{0.504}[PF_6]_{0.496}$ and $[N_{2222}][PF_6]$

	$[N_{2222}][BF_4]_{0.504}[PF_6]_{0.496}$	$[N_{2222}][PF_6]$
Formula	$C_8H_{20}B_{0.504}F_{4.992}NP_{0.496}$	$C_8H_{20}F_6NP$
Fw	245.90	404.39
crystal size, mm	0.40×0.40×0.60	0.10×0.30×0.40
T/K	223	298
crystal system	tetragonal	monoclinic
space group	$I-4$	$C2/c$
a/Å	9.324(2)	13.290(2)
b/Å	–	6.862(1)
c/Å	7.137(2)	13.353(2)
β/deg	–	92.855(5)
V/Å^3	620.5(2)	1217.5(3)
Z	2	4
ρ_{calcd}/g cm^{-3}	1.317	1.501
$2\theta_{max}$/deg	49.98	57.62
Data completeness	0.993	–
F(000)	260	–
μ/mm^{-1}	1.317	–
λ/Å	0.71073	0.71073
T_{min}/T_{max}	0.5291/1.000	–
No. reflns collected, unique	4770, 540	–
No. reflns in refinement	4770	–
No. parameters, restraints	50,24	–
R_{int}	0.0223	–
$R_1(F_o)^a$	0.0649	–
$wR_2(F_o^2)^b$	0.1880	–
Goodness-of-fit on F^2	1.159	–
Largest difference peak, hole / e Å^{-3}	0.244, −0.181	–
CCDC No.	1517064	–

^{a} $R_1 = \sum||F_o| - |F_c|| / \sum|F_o|$ for $I > 2\sigma(I)$. ^{b} $wR_2 = \{\sum[w(F_o^2 - F_c^2)^2] / \sum[w(F_o^2)^2]\}^{1/2}$ for $I > 2\sigma(I)$.

Table S2 Experimental and calculated XRD data and indices for the $[N_{2222}][BF_4]$–$[N_{2222}][PF_6]$ binary system.

$[N_{2222}][BF_4]$ (Phase I, 373 K)						
h	*k*	*l*	$d_{obs.}$ / Å	$d_{calc.}$ / Å	$2\theta_{obs.}$ / deg.	$2\theta_{calc.}$ / deg.
1	1	1	6.276	6.300	14.11	14.06
2	0	0	5.477	5.457	16.18	16.24
2	2	0	3.863	3.860	23.02	23.04
3	1	1	3.292	3.293	27.08	27.08
2	2	2	3.151	3.153	28.32	28.31
Cubic, a = 10.929(8), V = 1305.5(18)						

$[N_{2222}][BF_4]$:$[N_{2222}][PF_6]$ = 9:1 (Phase I, 373 K)						
h	*k*	*l*	$d_{obs.}$ / Å	$d_{calc.}$ / Å	$2\theta_{obs.}$ / deg.	$2\theta_{calc.}$ / deg.
1	1	1	6.311	6.326	14.03	14.00
2	0	0	5.490	5.479	16.14	16.18
2	2	0	3.876	3.874	22.94	22.96
3	1	1	3.304	3.304	26.98	26.99
2	2	2	3.162	3.163	28.22	28.21
Cubic, a = 10.959(5), V = 1316.2(11)						

$[N_{2222}][BF_4]$:$[N_{2222}][PF_6]$ = 8:2 (Phase I, 373 K)						
h	*k*	*l*	$d_{obs.}$ / Å	$d_{calc.}$ / Å	$2\theta_{obs.}$ / deg.	$2\theta_{calc.}$ / deg.
1	1	1	6.348	6.356	13.95	13.93
2	0	0	5.508	5.502	16.09	16.11
2	2	0	3.888	3.887	22.87	22.88
3	1	1	3.313	3.314	26.91	26.90
2	2	2	3.172	3.172	28.13	28.13
Cubic, a = 10.971(2), V = 1320.4(6)						

$[N_{2222}][BF_4]$:$[N_{2222}][PF_6]$ = 7:3 (Phase I, 373 K)						
h	*k*	*l*	$d_{obs.}$ / Å	$d_{calc.}$ / Å	$2\theta_{obs.}$ / deg.	$2\theta_{calc.}$ / deg.
1	1	1	6.3966	6.3990	13.84	13.84
2	0	0	5.5378	5.5367	16.00	16.01
2	2	0	3.9097	3.9084	22.74	22.75
3	1	1	3.3309	3.3311	26.76	26.76
2	2	2	3.1884	3.1888	27.98	27.98
Cubic, *a* = 11.0109(11), *V* = 1335.0(2)						

$[N_{2222}][BF_4]$:$[N_{2222}][PF_6]$ = 6:4 (Phase I, 373 K)						
h	*k*	*l*	$d_{obs.}$ / Å	$d_{calc.}$ / Å	$2\theta_{obs.}$ / deg.	$2\theta_{calc.}$ / deg.
1	1	1	6.3966	6.3998	13.84	13.84
2	0	0	5.5447	5.5414	15.98	15.99
2	2	0	3.9165	3.9170	22.70	22.70
3	1	1	3.3407	3.3400	26.68	26.69
2	2	2	3.1973	3.1978	27.90	27.90
Cubic, *a* = 11.0701(15), *V* = 1356.6(3)						

$[N_{2222}][BF_4]$:$[N_{2222}][PF_6]$ = 5:5 (Phase I, 373 K)						
h	*k*	*l*	$d_{obs.}$ / Å	$d_{calc.}$ / Å	$2\theta_{obs.}$ / deg.	$2\theta_{calc.}$ / deg.
1	1	1	6.434	6.427	13.76	13.78
2	0	0	5.558	5.564	15.94	15.93
2	2	0	3.930	3.930	22.62	22.62
3	1	1	3.351	3.351	26.60	26.60
2	2	2	3.209	3.208	27.80	27.81
Cubic, *a* = 11.094(2), *V* = 1365.3(4)						

$[N_{2222}][BF_4]$:$[N_{2222}][PF_6]$ = 4:6 (Phase I, 373 K)						
h	*k*	*l*	$d_{obs.}$ / Å	$d_{calc.}$ / Å	$2\theta_{obs.}$ / deg.	$2\theta_{calc.}$ / deg.
1	1	1	6.4616	6.4618	13.70	13.70
2	0	0	5.5933	5.5931	15.84	15.85
2	2	0	3.9508	3.9509	22.50	22.50
3	1	1	3.3679	3.3681	26.46	26.46
2	2	2	3.2245	3.2244	27.66	27.67
Cubic, *a* = 11.1481(2), *V* = 1385.48(4)						

$[N_{2222}][BF_4]$:$[N_{2222}][PF_6]$ = 3:7 (Phase I, 373 K)						
h	*k*	*l*	$d_{obs.}$ / Å	$d_{calc.}$ / Å	$2\theta_{obs.}$ / deg.	$2\theta_{calc.}$ / deg.
1	1	1	6.4616	6.4599	13.70	13.71
2	0	0	5.5933	5.5952	15.84	15.84
2	2	0	3.9578	3.9574	22.46	22.47
3	1	1	3.3754	3.3752	26.40	26.41
2	2	2	3.2314	3.2316	27.60	27.60
Cubic, *a* = 11.2001(8), *V* = 1404.97(17)						

$[N_{2222}][BF_4]$:$[N_{2222}][PF_6]$ = 2:8 (Phase I, 373 K)						
h	*k*	*l*	$d_{obs.}$ / Å	$d_{calc.}$ / Å	$2\theta_{obs.}$ / deg.	$2\theta_{calc.}$ / deg.
1	1	1	6.518	6.517	13.58	13.59
2	0	0	5.636	5.640	15.72	15.71
2	2	0	3.986	3.982	22.30	22.32
3	1	1	3.396	3.395	26.24	26.25
2	2	2	3.248	3.250	27.46	27.45
Cubic, *a* = 11.227(3), *V* = 1415.2(7)						

$[N_{2222}][BF_4]$:$[N_{2222}][PF_6]$ = 1:9 (Phase I, 373 K)						
h	*k*	*l*	$d_{obs.}$ / Å	$d_{calc.}$ / Å	$2\theta_{obs.}$ / deg.	$2\theta_{calc.}$ / deg.
1	1	1	6.5376	6.5368	13.54	13.55
2	0	0	5.6572	5.6589	15.66	15.66
2	2	0	4.0000	3.9986	22.22	22.23
3	1	1	3.4084	3.4091	26.14	26.14
2	2	2	3.2639	3.2638	27.32	27.33
Cubic, *a* = 11.2907(12), *V* = 1439.3(2)						

$[N_{2222}][PF_6]$ (Phase I, 373 K)						
h	*k*	*l*	$d_{obs.}$ / Å	$d_{calc.}$ / Å	$2\theta_{obs.}$ / deg.	$2\theta_{calc.}$ / deg.
1	1	1	6.5472	6.5491	13.52	13.52
2	0	0	5.6716	5.6700	15.62	15.63
2	2	0	4.0071	4.0070	22.18	22.19
3	1	1	3.4161	3.4164	26.08	26.08
2	2	2	3.2709	3.2708	27.26	27.27
Cubic, *a* = 11.3179(7), *V* = 1449.78(16)						

Table S2 Raman data for $\nu_s(NC_4)$ in $[N_{2222}][BF_4]$.

	Temperature / K	Conformation	Raman shift	FWHM
$[N_{2222}][BF_4]$ (Transition point: 340 K)				
	373	*TT*	671.8	3.1
	348	*TT*	672.0	3.1
	333	*TG*	660.9	3.2
	313	*TG*	661.3	3.0
	298	*TG*	661.6	3.0

Lorentz function: $f(x) = h/\{1+(x-u)^2/w^2\}+b$
h = peak intensity, u = peak position, w = full width at half maximum, b = background

Table S3 Raman data for $\nu_s(NC_4)$ in $[N_{2222}][BF_4]$−$[N_{2222}][PF_6]$ = 5:5.

	Temperature / K	Conformation	Raman shift	FWHM
$[N_{2222}][BF_4]$ – $[N_{2222}][PF_6]$ = 5:5 (Transition point: 323 K)				
	373	*TT*	671.1	2.7
	348	*TT*	671.6	2.8
	333	*TT*	671.8	3.0
	313	*TG / TT*	659.7 / 672.0	3.6 / 2.5
	298	*TG*	659.9	2.8

Lorentz function: $f(x) = h/\{1+(x-u)^2/w^2\}+b$
h = peak intensity, u = peak position, w = full width at half maximum, b = background

Table S4 Raman data for $\nu_s(NC_4)$ in $[N_{2222}][PF_6]$.

	Temperature / K	Conformation	Raman shift	FWHM
$[N_{2222}][PF_6]$ (Transition point: 345 K)				
	373	*TT*	671.5	3.2
	348	*TT*	671.8	3.0
	333	*TG*	659.7	3.3
	313	*TG*	660.0	3.2
	298	*TG*	660.0	3.1

Lorentz function: $f(x) = h/\{1+(x-u)^2/w^2\}+b$
h = peak intensity, u = peak position, w = full width at half maximum, b = background

Table S5 Raman data for $\nu_1(BF_4^-)$ in $[N_{2222}][BF_4]$.

Temperature / K	Mode	Raman shift	FWHM
$[N_{2222}][BF_4]$ (Transition point: 340 K)			
373	$\nu_1(BF_4^-)$	762.4	1.5
348	$\nu_1(BF_4^-)$	762.5	1.4
333	$\nu_1(BF_4^-)$	764.4	1.3
313	$\nu_1(BF_4^-)$	764.6	1.2
298	$\nu_1(BF_4^-)$	764.7	1.4

Lorentz function: $f(x) = h/\{1+(x-u)^2/w^2\}+b$
h = peak intensity, u = peak position, w = full width at half maximum, b = background

Table S6 Raman data for $\nu_1(BF_4^-)$ and $\nu_1(PF_6^-)$ in the $[N_{2222}][BF_4]$−$[N_{2222}][PF_6]$ = 5:5.

Temperature / K	Mode	Raman shift	FWHM
$[N_{2222}][BF_4]$ – $[N_{2222}][PF_6]$ = 5:5 (Transition point: 323 K)			
373	$\nu_1(PF_6^-)$ / $\nu_1(BF_4^-)$	739.2 / 761.7	1.9 / 1.4
348	$\nu_1(PF_6^-)$ / $\nu_1(BF_4^-)$	739.6 / 762.0	1.8 / 1.4
333	$\nu_1(PF_6^-)$ / $\nu_1(BF_4^-)$	739.7 / 762.0	1.8 / 1.4
313	$\nu_1(PF_6^-)$ / $\nu_1(BF_4^-)$	741.0 / 762.5	2.2 / 1.4
298	$\nu_1(PF_6^-)$ / $\nu_1(BF_4^-)$	742.7 / 763.3	1.7 / 1.3

Lorentz function: $f(x) = h/\{1+(x-u)^2/w^2\}+b$
h = peak intensity, u = peak position, w = full width at half maximum, b = background

Table S7 Raman data for $\nu_1(PF_6^-)$ in $[N_{2222}][PF_6]$.

Temperature / K	Mode	Raman shift	FWHM
$[N_{2222}][PF_6]$ (Transition point: 345 K)			
373	$\nu_1(PF_6^-)$	739.8	1.9
348	$\nu_1(PF_6^-)$	740.0	1.9
333	$\nu_1(PF_6^-)$	741.1	1.7
313	$\nu_1(PF_6^-)$	741.5	1.7
298	$\nu_1(PF_6^-)$	741.5	1.7

Lorentz function: $f(x) = h/\{1+(x-u)^2/w^2\}+b$
h = peak intensity, u = peak position, w = full width at half maximum, b = background

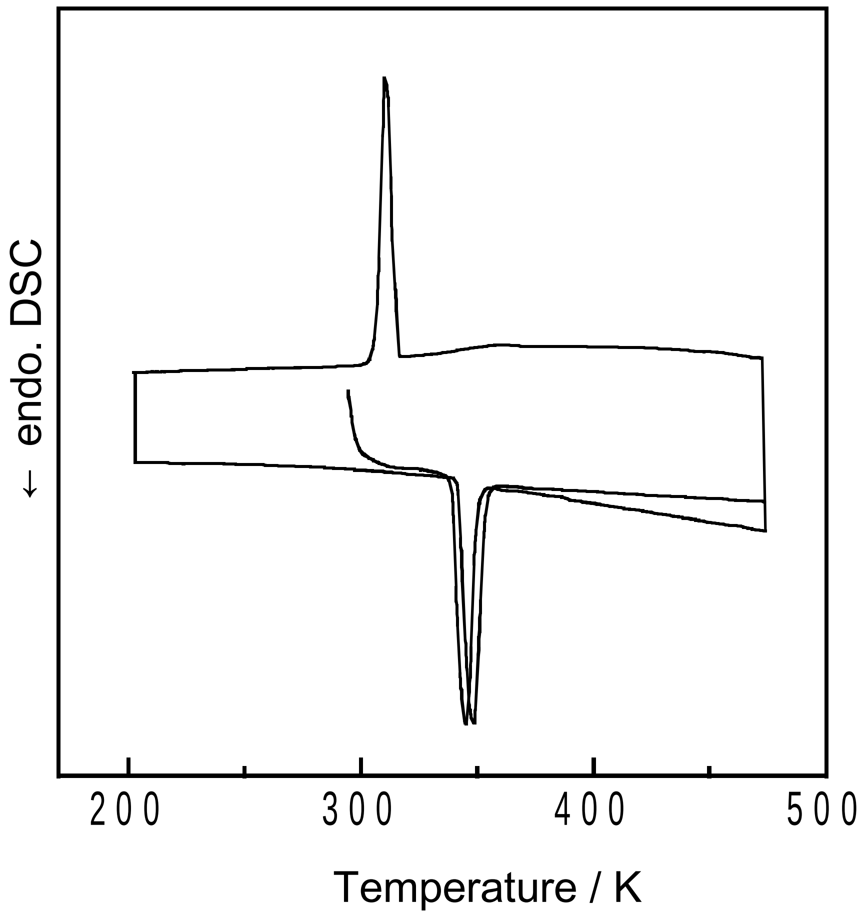

Fig. S1 Differential scanning calorimetric curve for $[N_{2222}][BF_4]$. Scan rate: 5 K min^{-1}

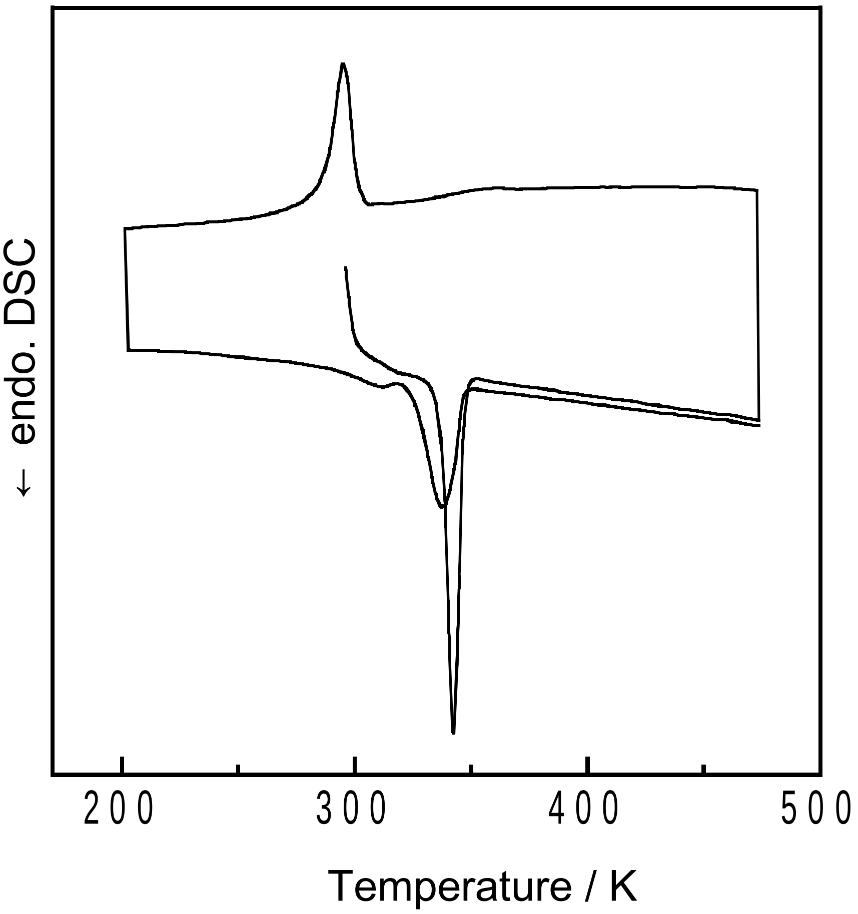

Fig. S2 Differential scanning calorimetric curve for $[N_{2222}][BF_4]$ − $[N_{2222}][PF_6]$ = 9:1. Scan rate: 5 K min^{-1}

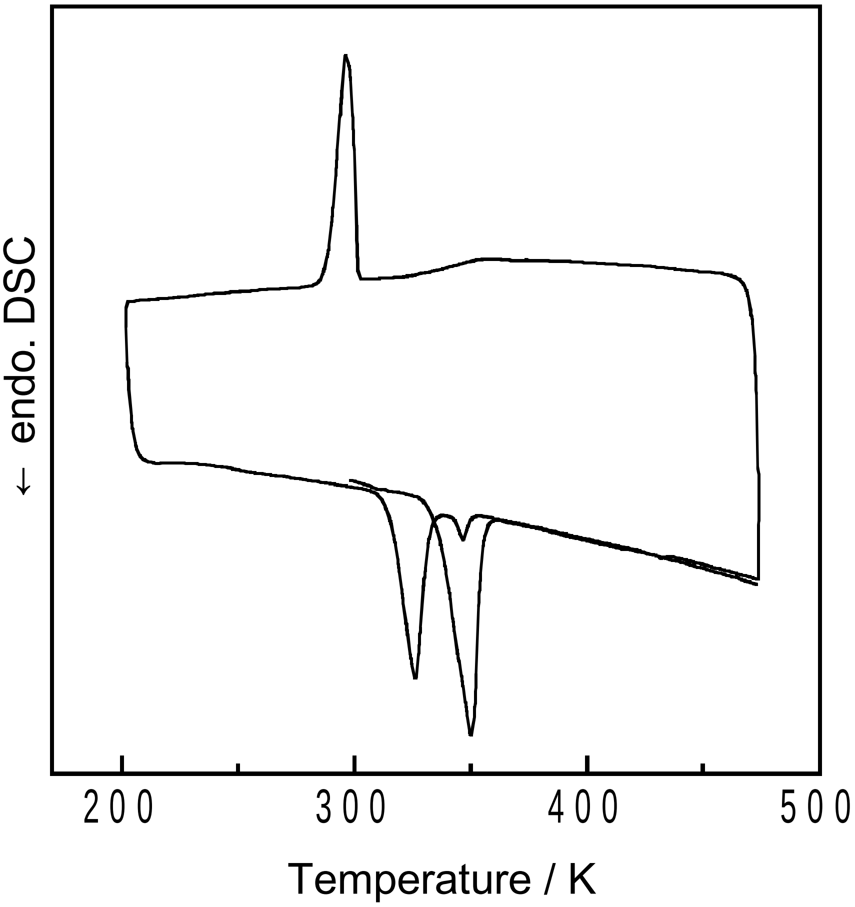

Fig. S3 Differential scanning calorimetric curve for $[N_{2222}][BF_4]$ − $[N_{2222}][PF_6]$ = 8:2. Scan rate: 5 K min^{-1}

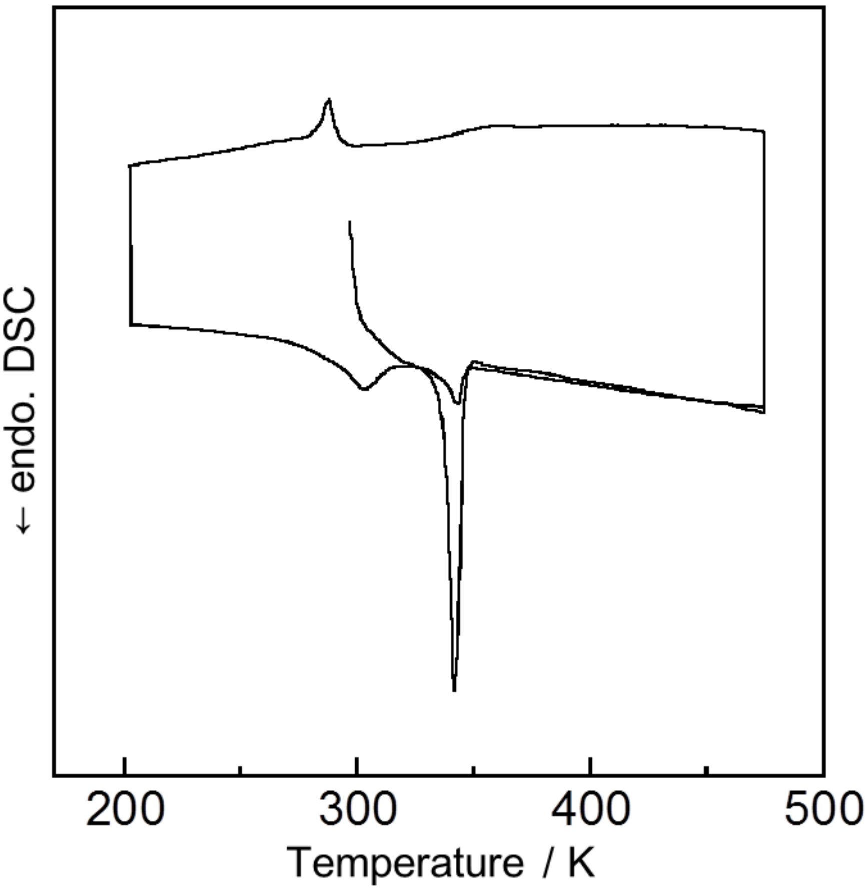

Fig. S4 Differential scanning calorimetric curve for $[N_{2222}][BF_4]$ – $[N_{2222}][PF_6]$ = 7:3. Scan rate: 5 K min^{-1}

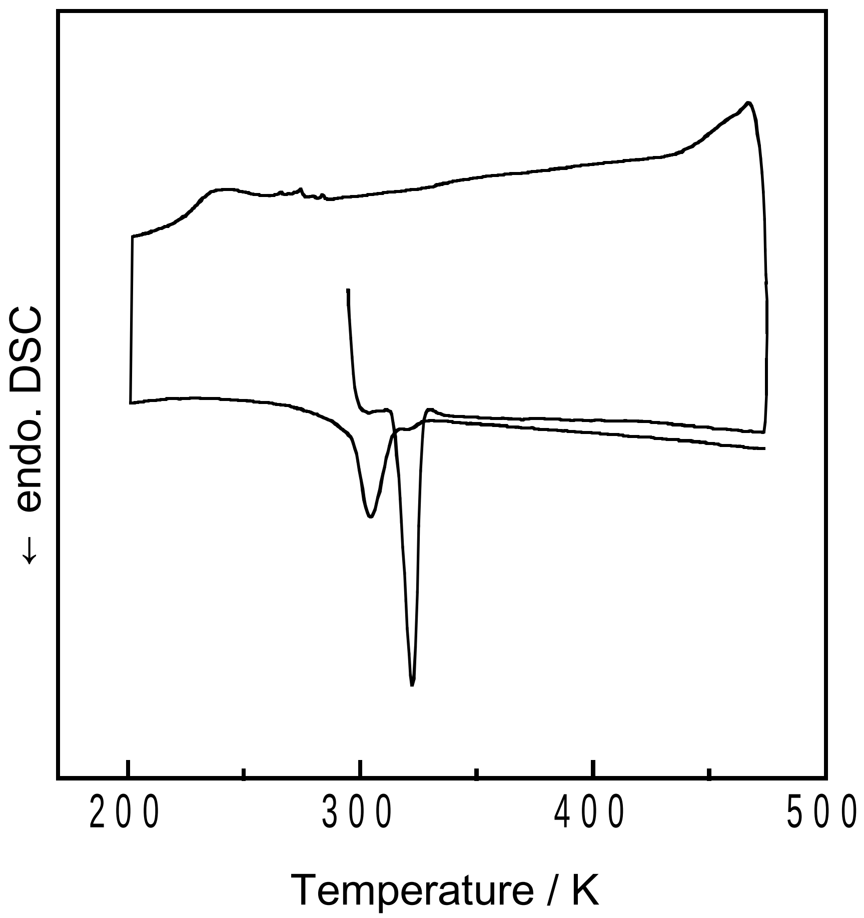

Fig. S5 Differential scanning calorimetric curve for $[N_{2222}][BF_4]$ – $[N_{2222}][PF_6]$ = 6:4. Scan rate: 5 K min^{-1}

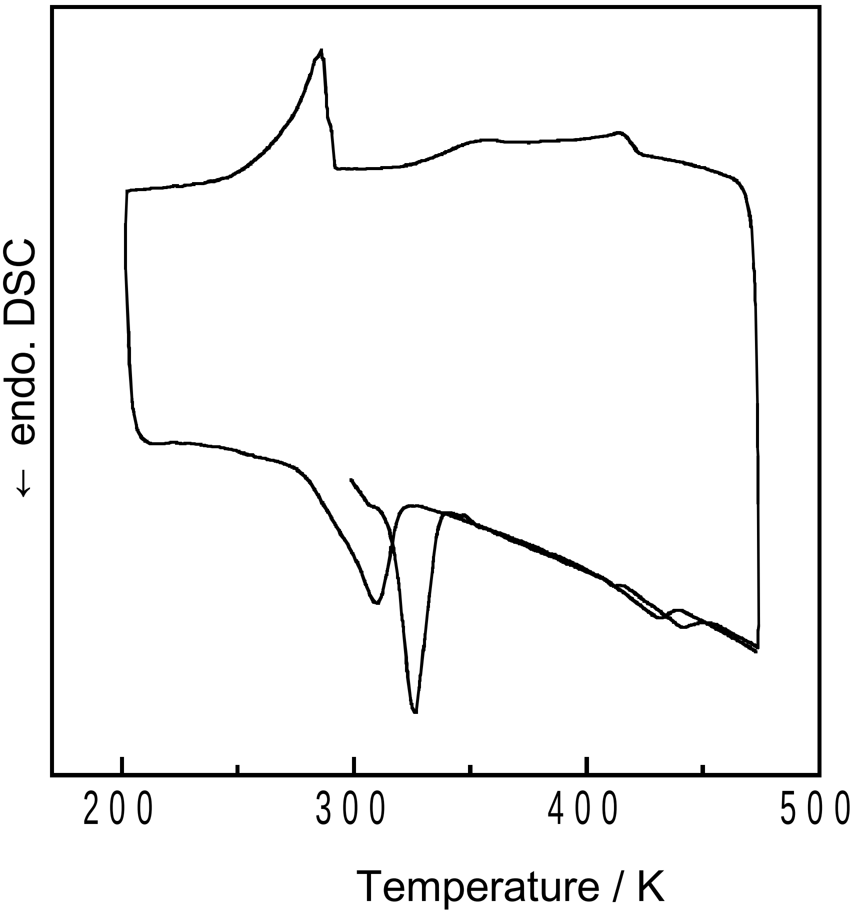

Fig. S6 Differential scanning calorimetric curve for $[N_{2222}][BF_4]$ – $[N_{2222}][PF_6]$ = 5:5. Scan rate: 5 K min^{-1}

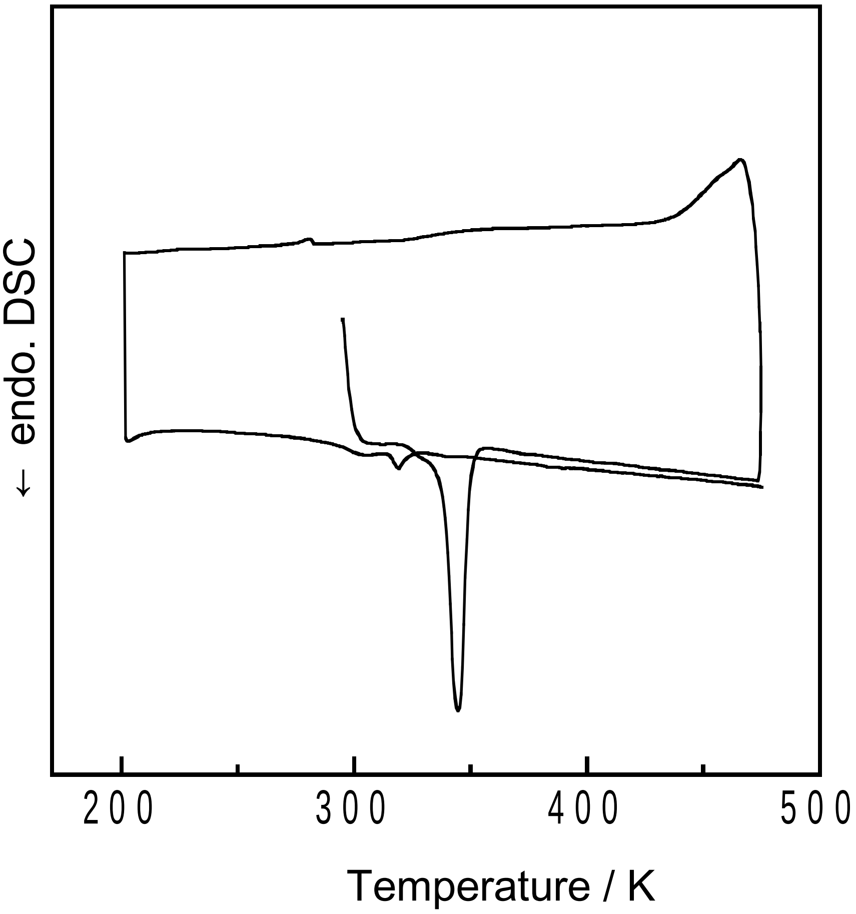

Fig. S7 Differential scanning calorimetric curve for $[N_{2222}][BF_4]$ – $[N_{2222}][PF_6]$ = 4:6. Scan rate: 5 K min^{-1}

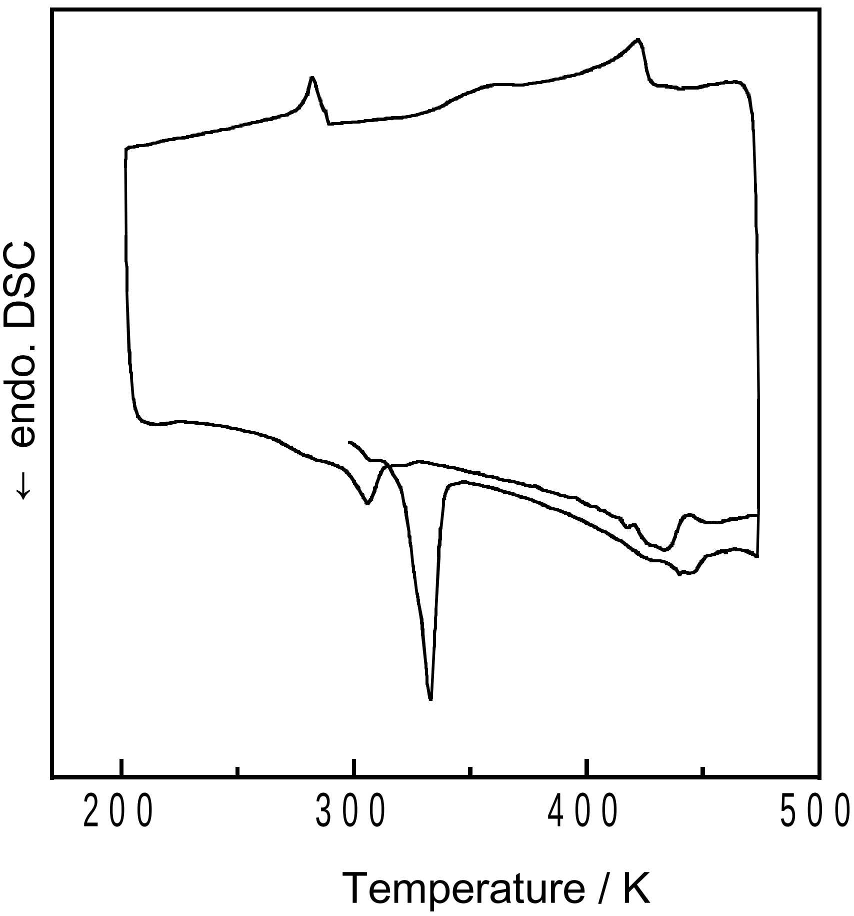

Fig. S8 Differential scanning calorimetric curve for $[N_{2222}][BF_4]$ – $[N_{2222}][PF_6]$ = 3:7. Scan rate: 5 K min^{-1}. The endothermic peak around 440 K is considered as artifact.

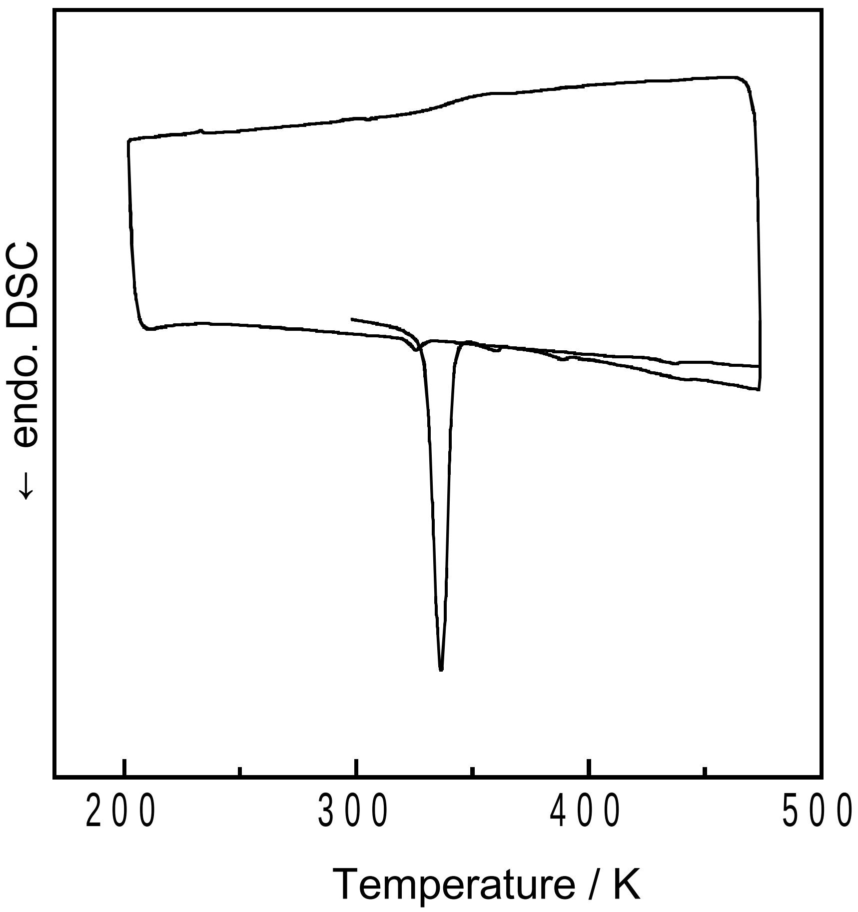

Fig. S9 Differential scanning calorimetric curve for $[N_{2222}][BF_4]$ − $[N_{2222}][PF_6]$ = 2:8. Scan rate: 5 K min^{-1}

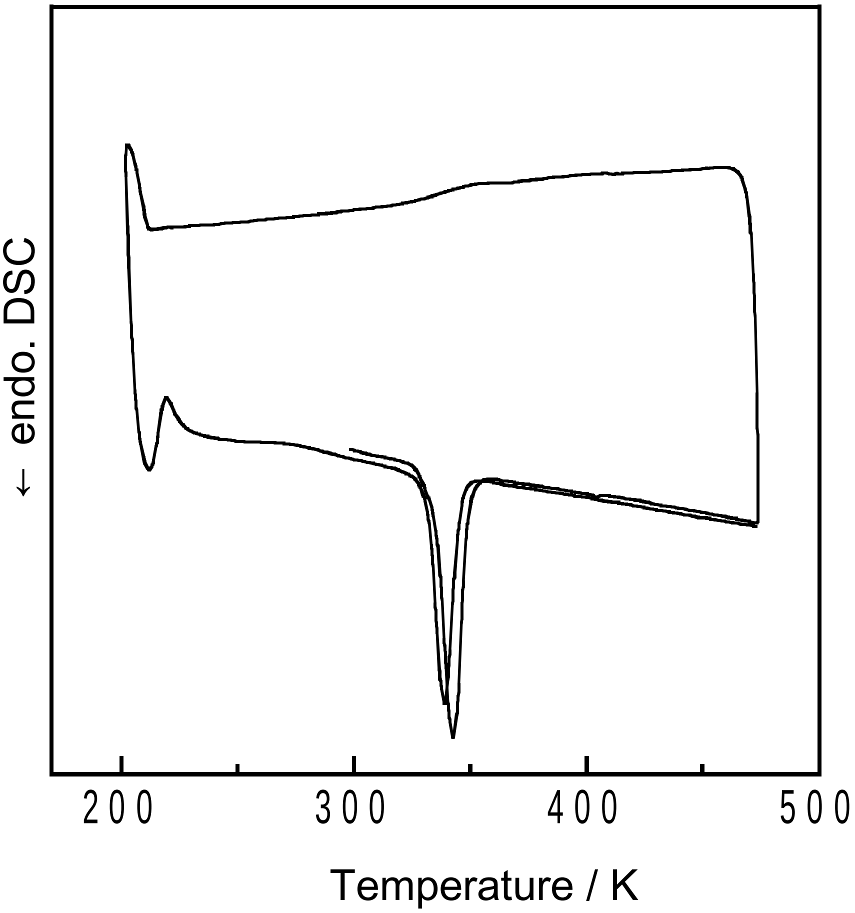

Fig. S10 Differential scanning calorimetric curve for $[N_{2222}][BF_4]$ − $[N_{2222}][PF_6]$ = 1:9. Scan rate: 5 K min^{-1}

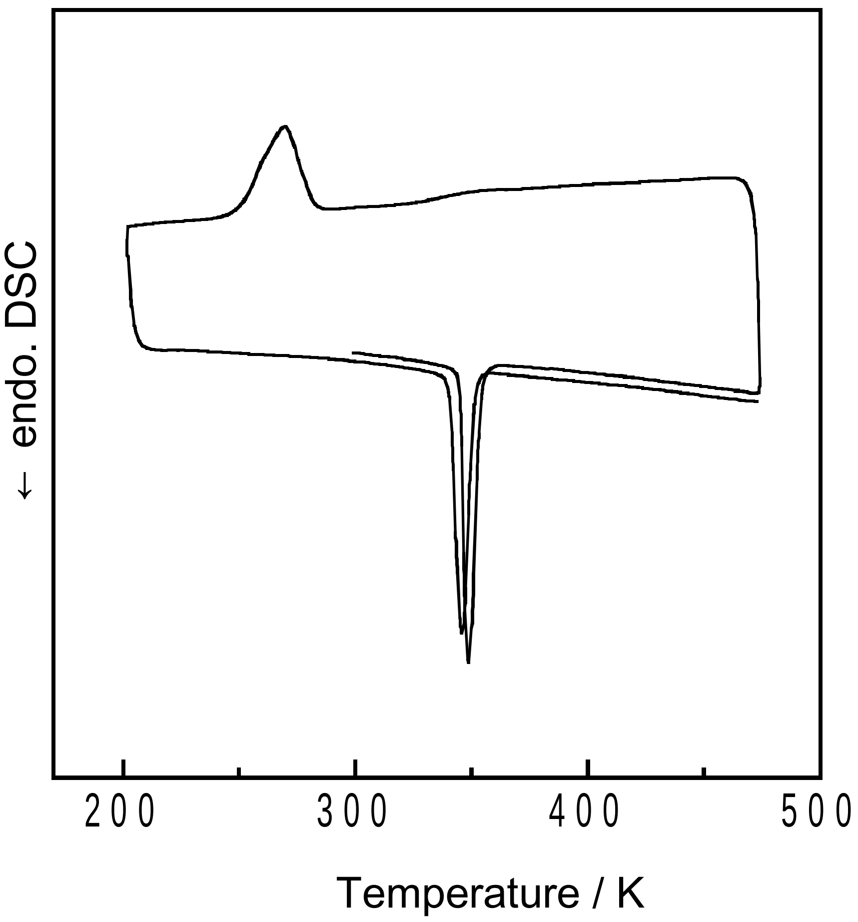

Fig. S11 Differential scanning calorimetric curve for $[N_{2222}][PF_6]$. Scan rate: 5 K min^{-1}

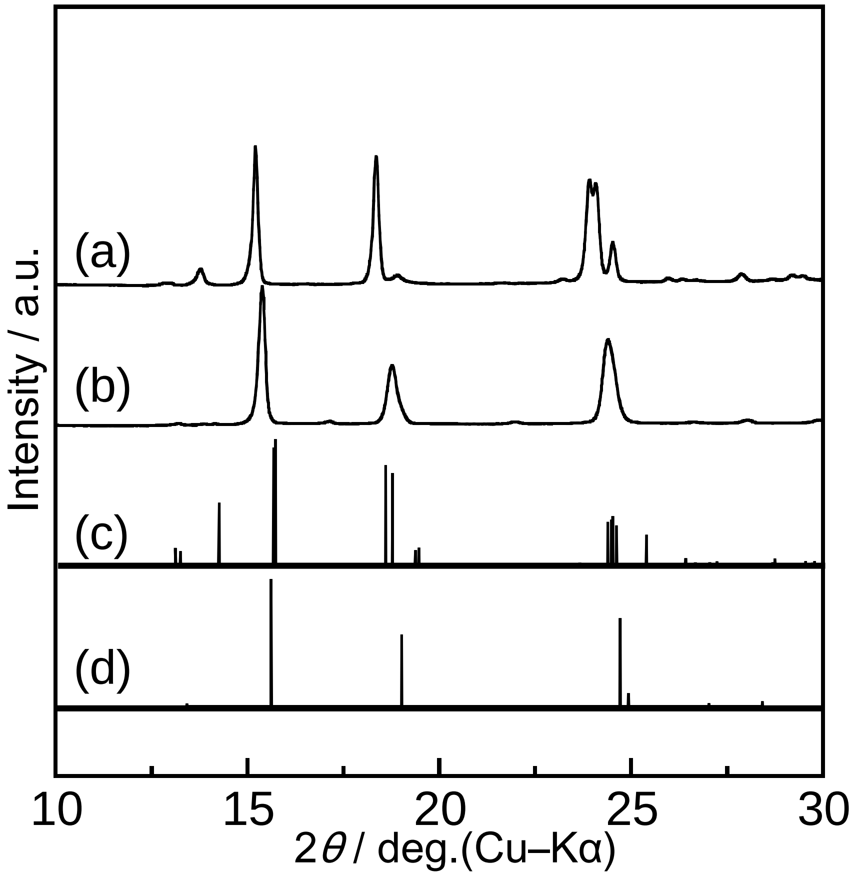

Fig. S12 X-ray diffraction patterns of (a) $[N_{2222}][PF_6]$ obtained 298 K, (b) $[N_{2222}][BF_4]$:$[N_{2222}][PF_6]$ = 5:5 obtained at 298 K, (c) $[N_{2222}][PF_6]$ simulated from the crystal structured determined at 220 K,[1] and (d) simulated $[N_{2222}][BF_4]_{0.504}[N_{2222}][PF_6]_{0.496}$ simulated from the crystal structure determined at 223 K. The pattern (b) is well reproduced by the pattern (d) by considering the lattice expansion from 223 K to 298 K.

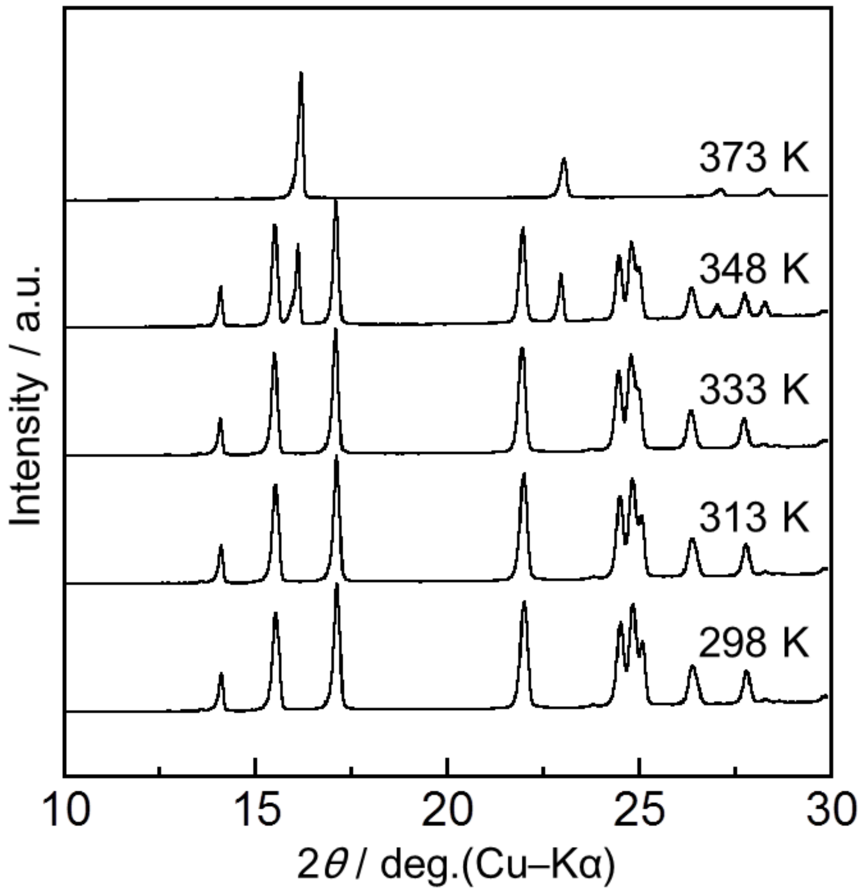

Fig. S13 Powder XRD patterns of $[N_{2222}][BF_4]$ at 298 K, 313 K, 333 K, 348 K, and 373 K.

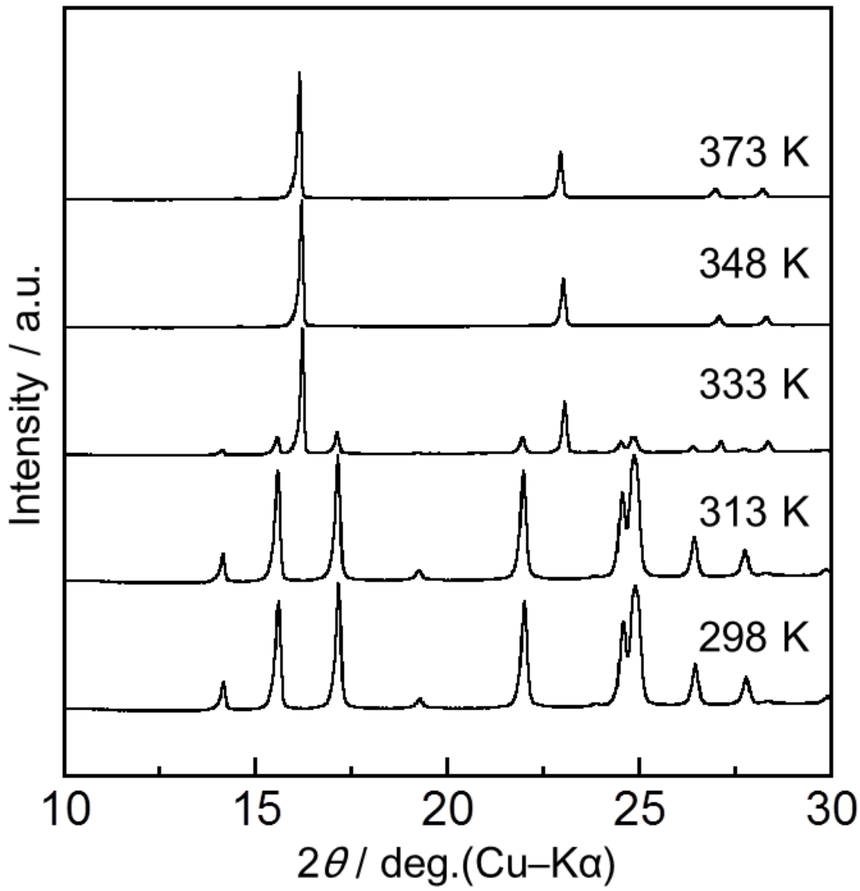

Fig. S14 Powder XRD patterns of $[N_{2222}][BF_4]$:$[N_{2222}][PF_6]$ = 9:1 at 298 K, 313 K, 333 K, 348 K, and 373 K.

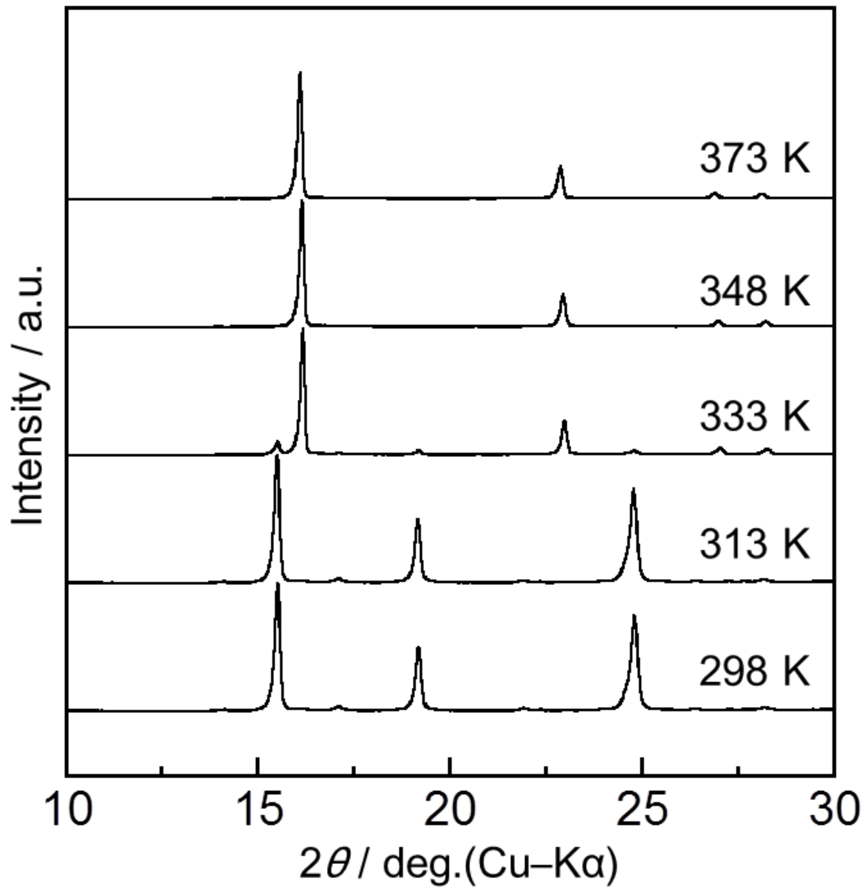

Fig. S15 Powder XRD patterns of $[N_{2222}][BF_4]$:$[N_{2222}][PF_6]$ = 8:2 at 298 K, 313 K, 333 K, 348 K, and 373 K.

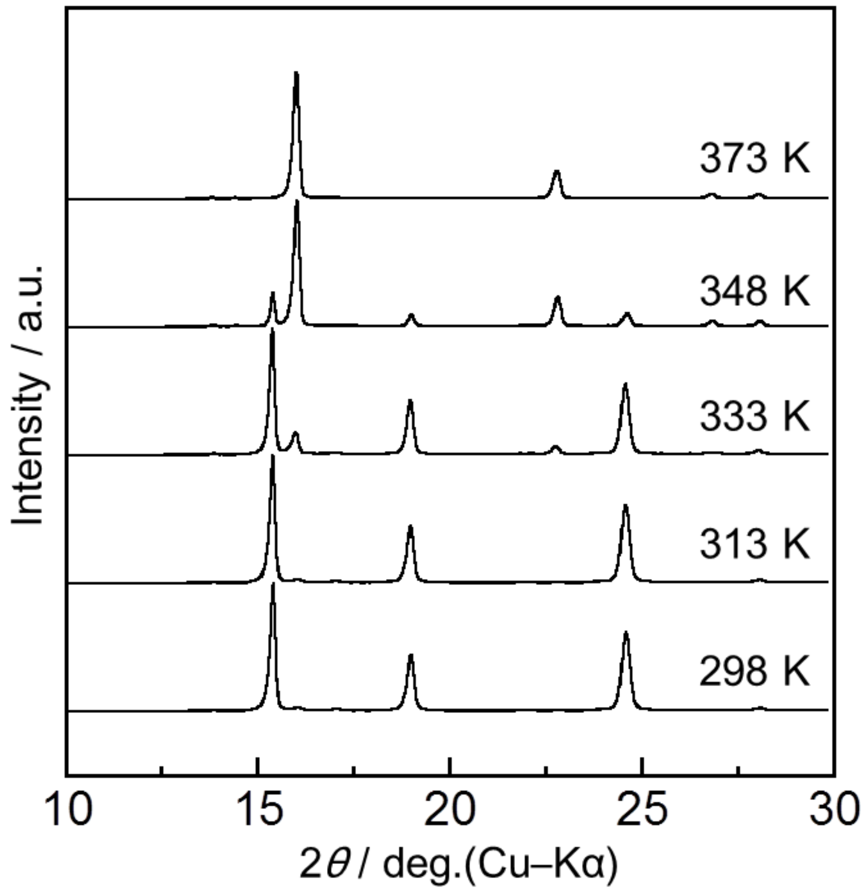

Fig. S16 Powder XRD patterns of $[N_{2222}][BF_4]$:$[N_{2222}][PF_6]$ = 7:3 at 298 K, 313 K, 333 K, 348 K, and 373 K.

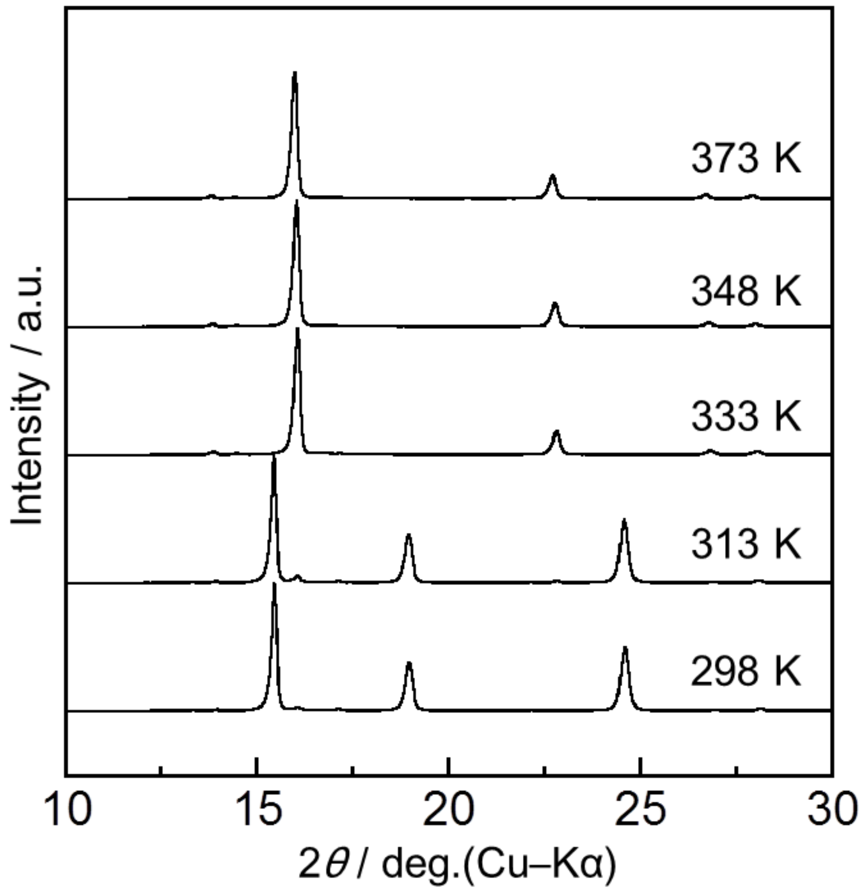

Fig. S17 Powder XRD patterns of $[N_{2222}][BF_4]$:$[N_{2222}][PF_6]$ = 6:4 at 298 K, 313 K, 333 K, 348 K, and 373 K.

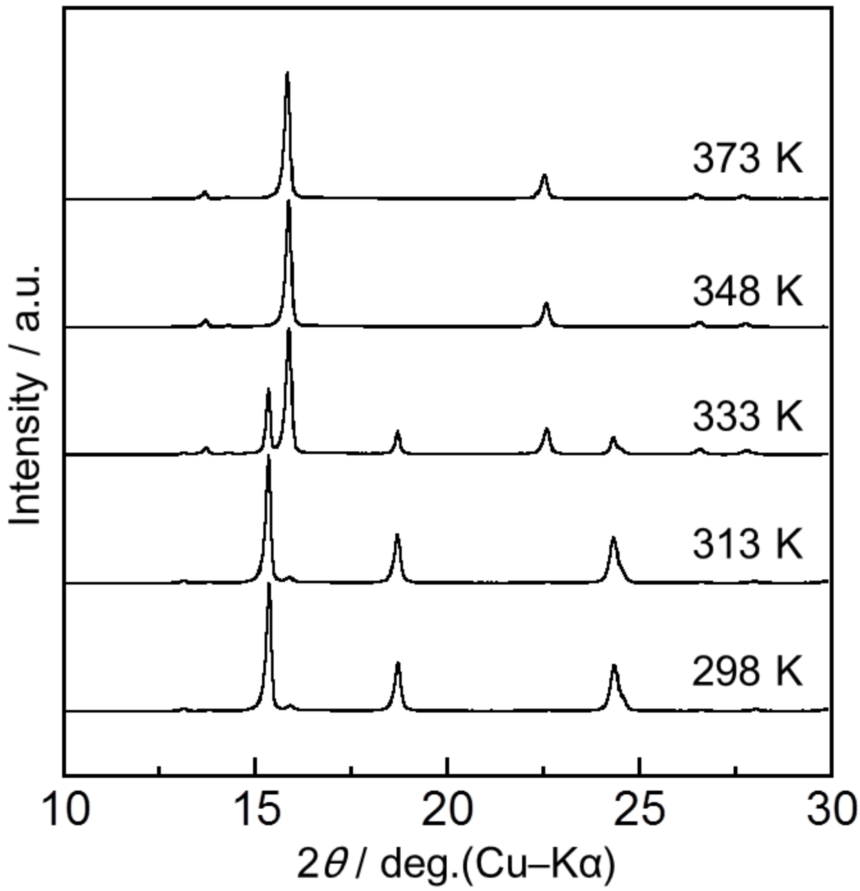

Fig. S18 Powder XRD patterns of $[N_{2222}][BF_4]$:$[N_{2222}][PF_6]$ = 4:6 at 298 K, 313 K, 333 K, 348 K, and 373 K.

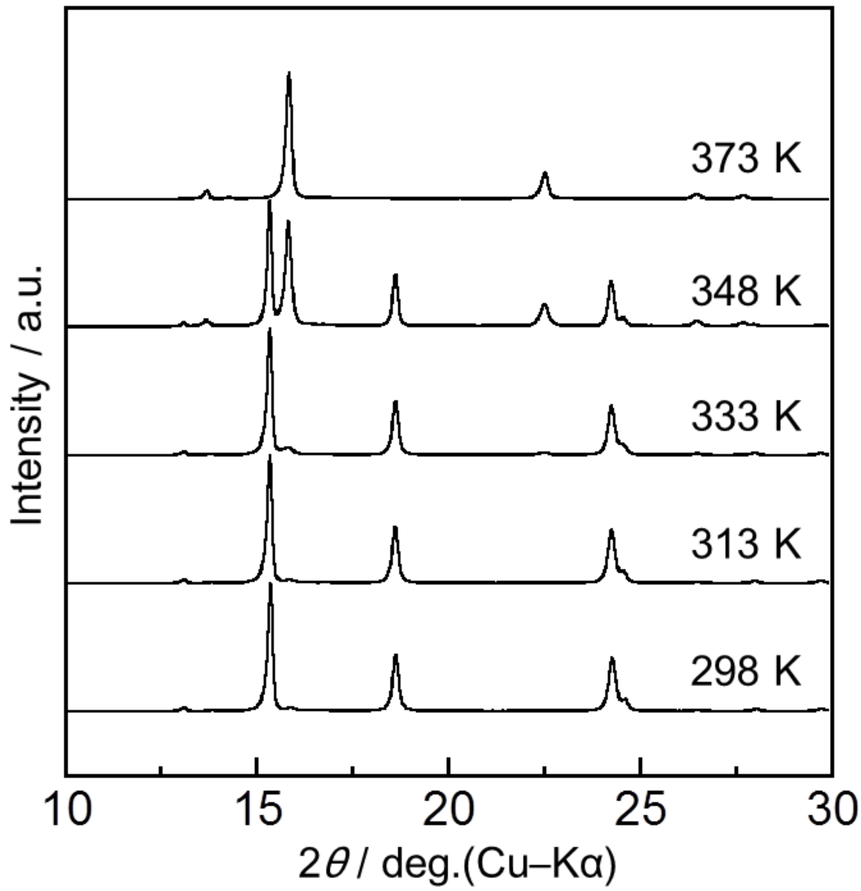

Fig. S19 Powder XRD patterns of $[N_{2222}][BF_4]$:$[N_{2222}][PF_6]$ = 3:7 at 298 K, 313 K, 333 K, 348 K, and 373 K.

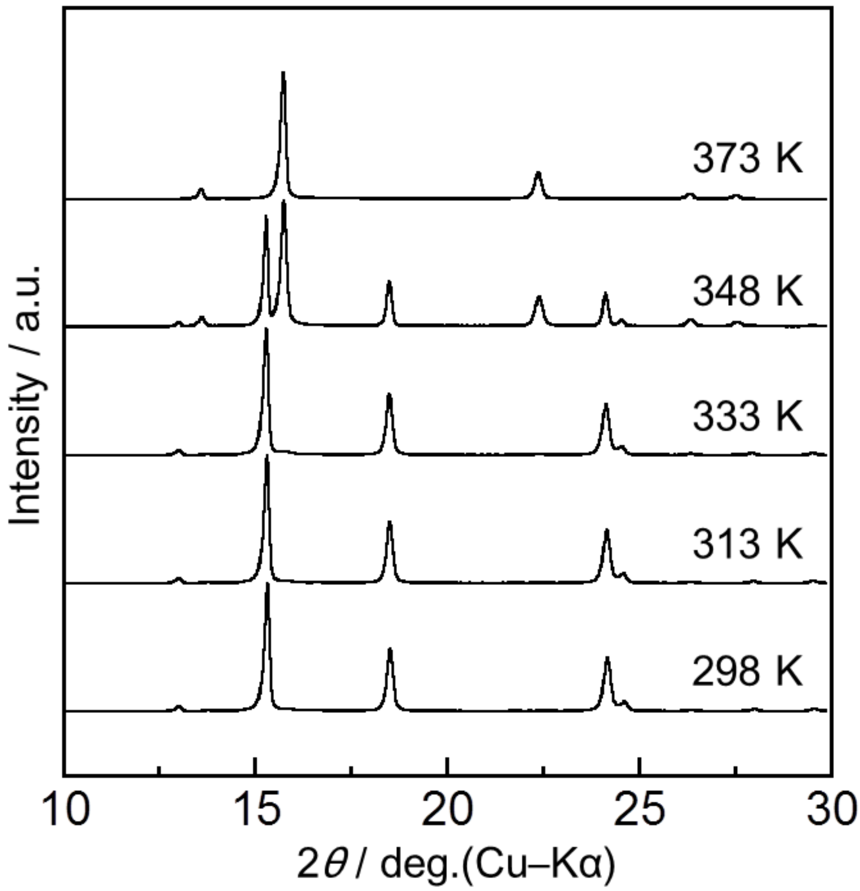

Fig. S20 Powder XRD patterns of $[N_{2222}][BF_4]$:$[N_{2222}][PF_6]$ = 2:8 at 298 K, 313 K, 333 K, 348 K, and 373 K.

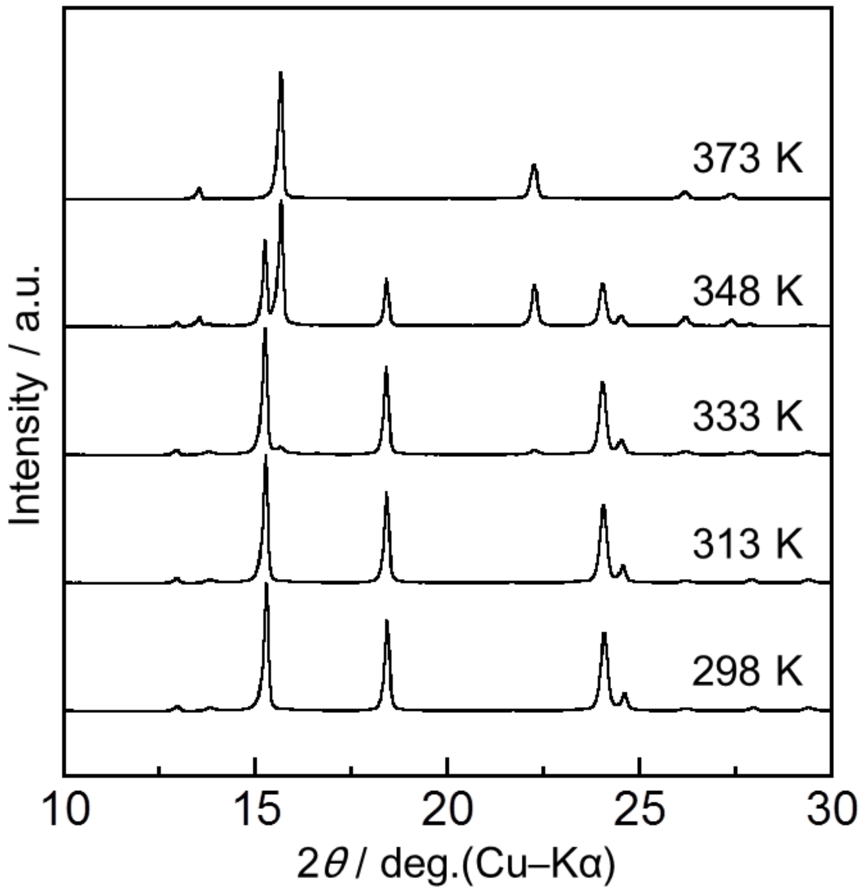

Fig. S21 Powder XRD patterns of $[N_{2222}][BF_4]$:$[N_{2222}][PF_6]$ = 1:9 at 298 K, 313 K, 333 K, 348 K, and 373 K.

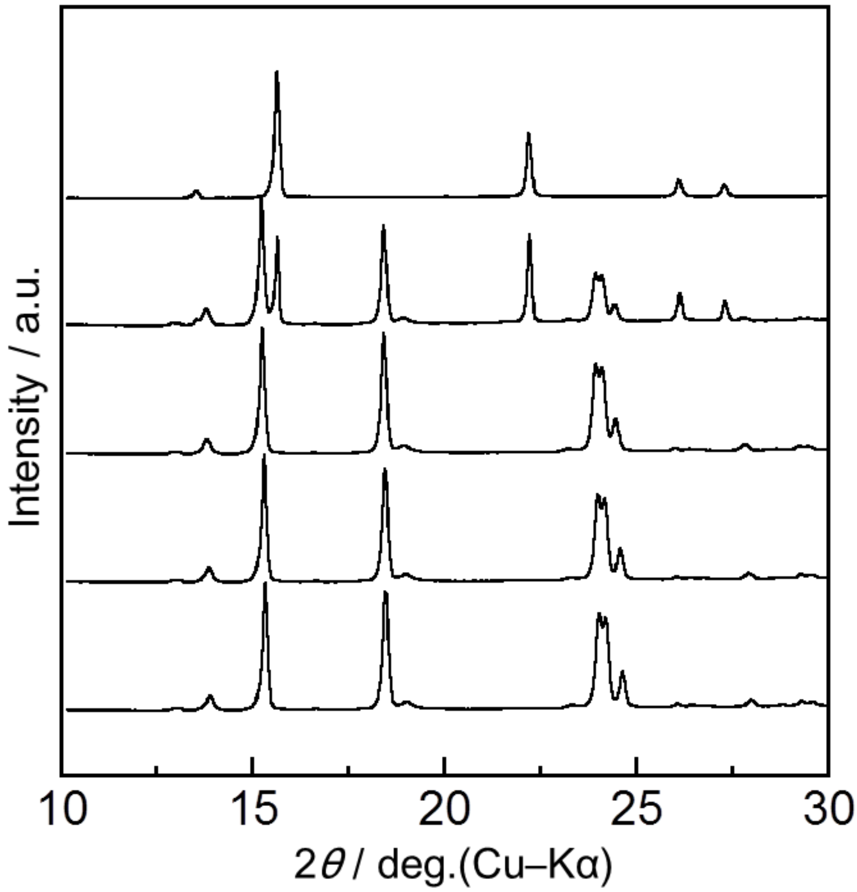

Fig. S22 Powder XRD patterns of $[N_{2222}][PF_6]$ at 298 K, 313 K, 333 K, 348 K, and 373 K.

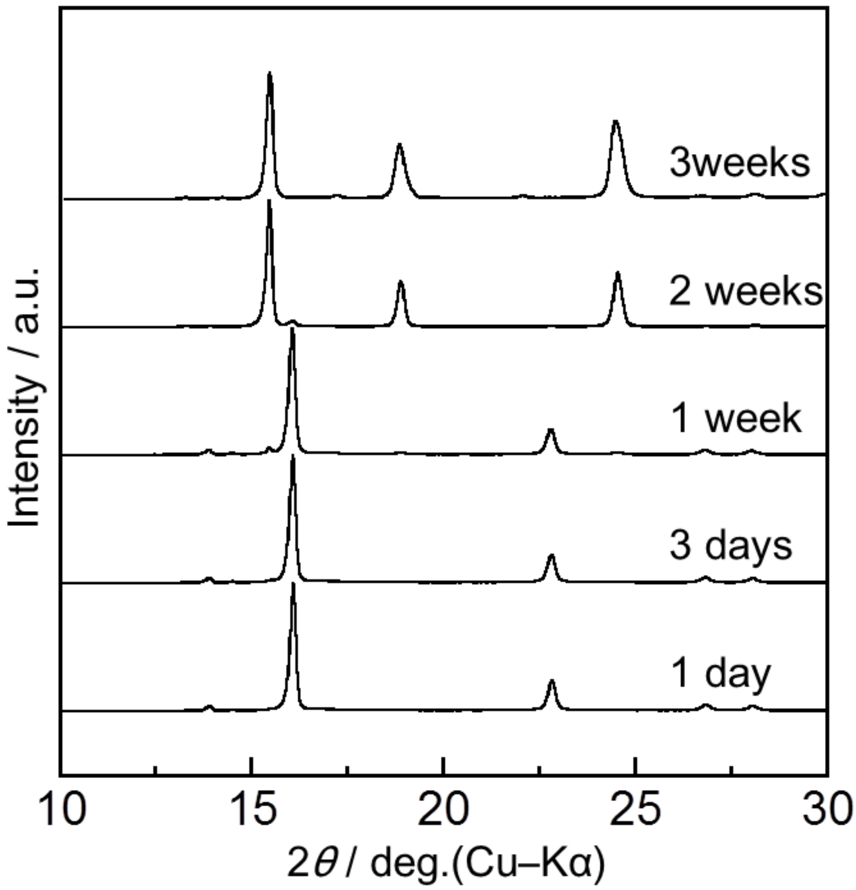

Fig. S23 Powder XRD patterns of $[N_{2222}][BF_4]$:$[N_{2222}][PF_6]$ = 5:5 at 298 K measured 1 day, 3 days, 1 week, 2 weeks, and 3 weeks after heat treatment at 473 K.

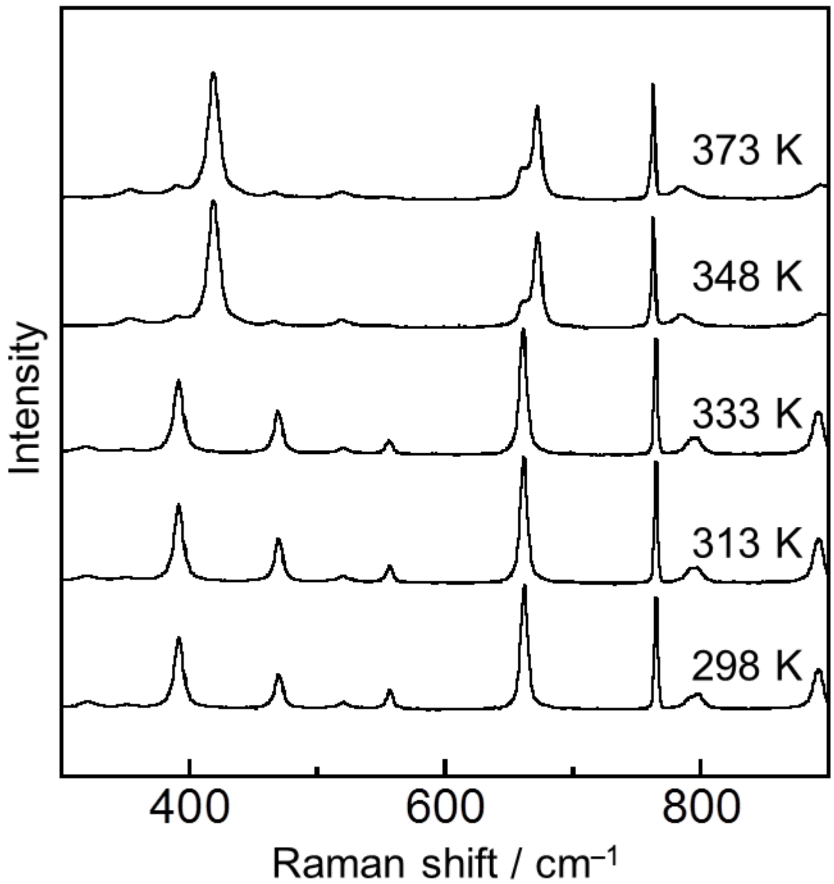

Fig. S24 Raman spectra for $[N_{2222}][BF_4]$ at 298 K, 313 K, 333 K, 348 K, and 373 K.

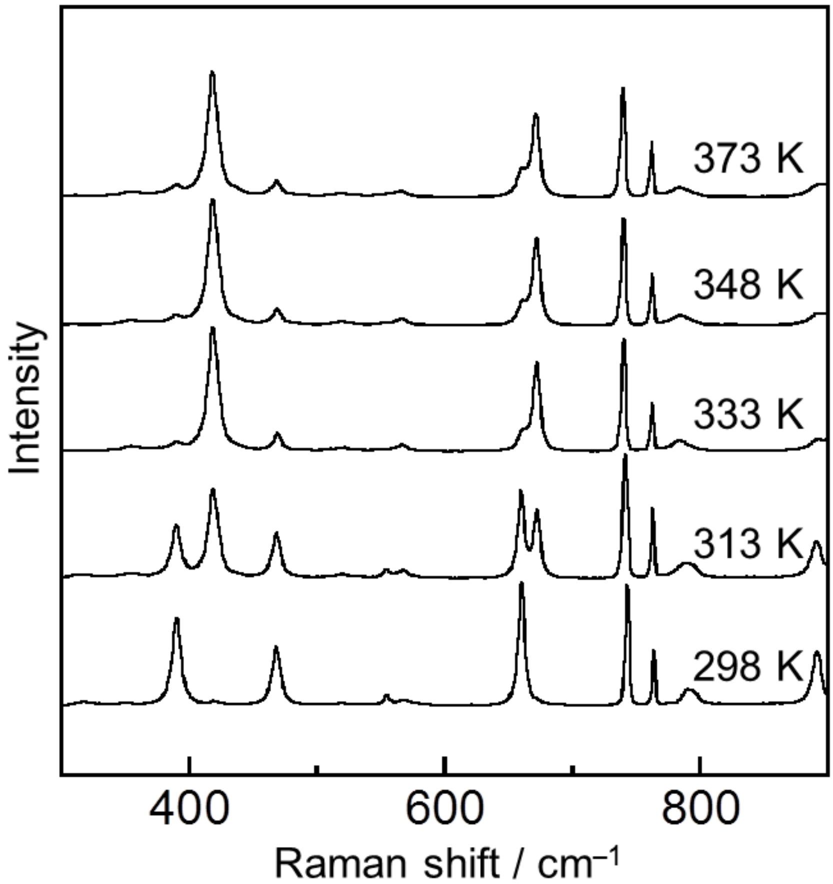

Fig. S25 Raman spectra for $[N_{2222}][BF_4]$:$[N_{2222}][PF_6]$ = 5:5 at 298 K, 313 K, 333 K, 348 K, and 373 K.

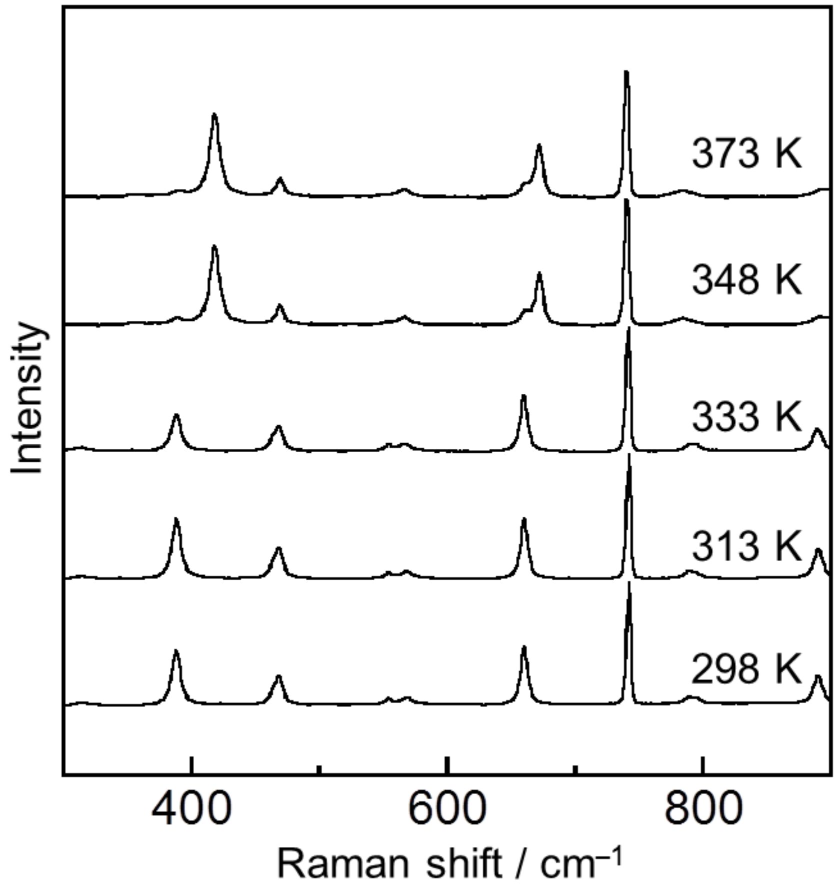

Fig. S26 Raman spectra for $[N_{2222}][PF_6]$ at 298 K, 313 K, 333 K, 348 K, and 373 K.

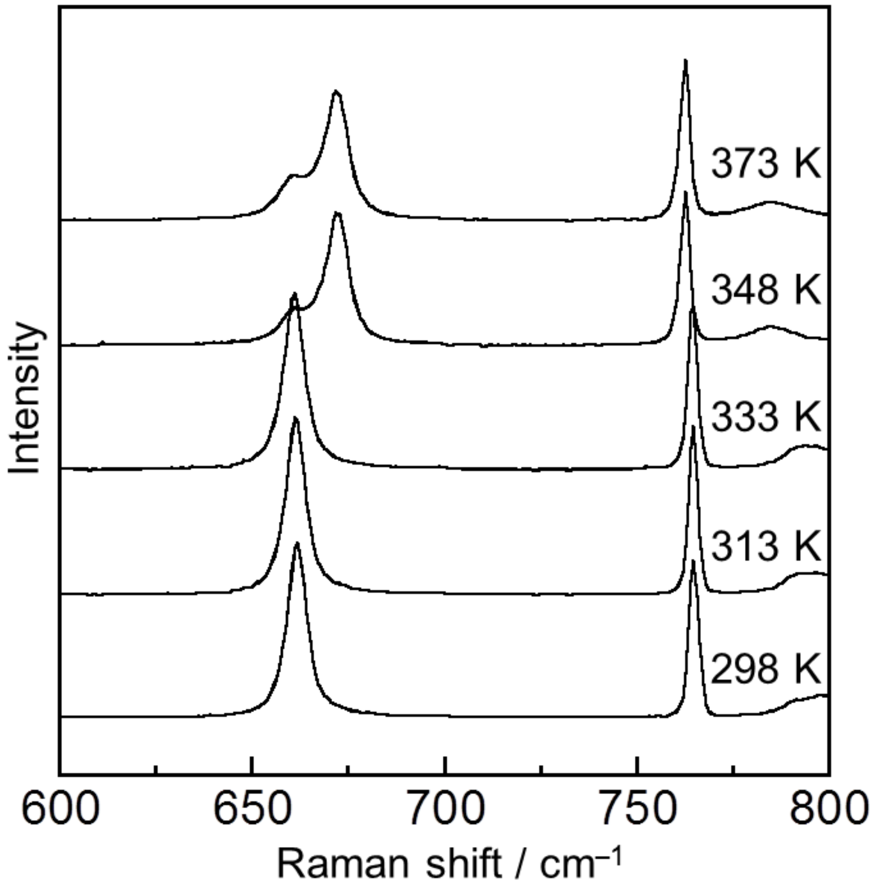

Fig. S27 Raman spectra in the range of 600−800 cm^{-1} for [N_{2222}][BF_4] at 298 K, 313 K, 333 K, 348 K, and 373 K.

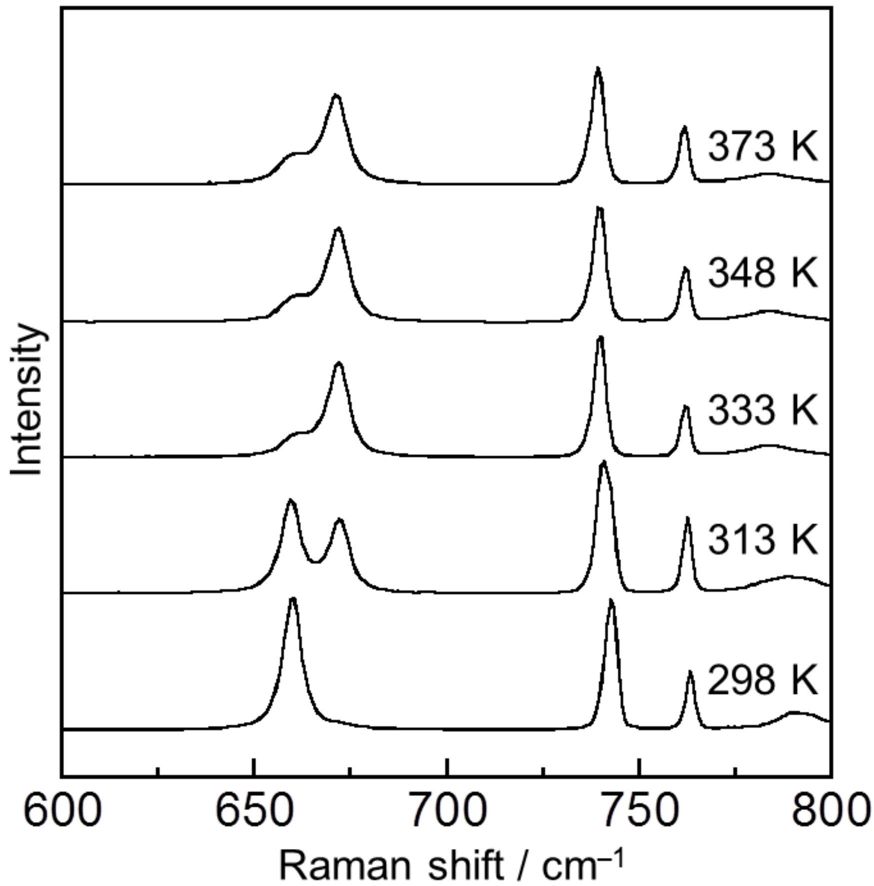

Fig. S28 Raman spectra in the range of 600 − 800 cm^{-1} for $[N_{2222}][BF_4]$:$[N_{2222}][PF_6]$ = 5:5 at 298 K, 313 K, 333 K, 348 K, and 373 K.

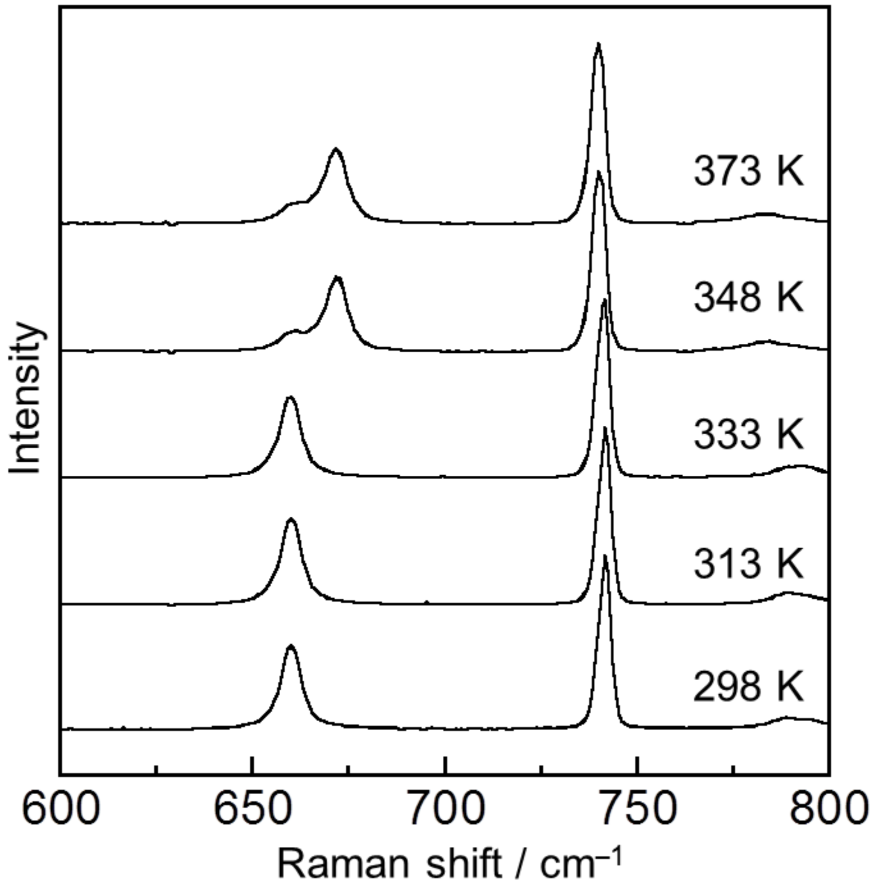

Fig. S29 Raman spectra in the range of 600−800 cm^{-1} for $[N_{2222}][PF_6]$ at 298 K, 313 K, 333 K, 348 K, and 373 K.

References

1. W. Beichel, U. P. Preiss, B. Benkmil, G. Steinfeld, P. Eiden, A. Kraft and I. Krossing, *Z. Anorg. Allg. Chem.*, 2013, **639**, 2153-2161.